JACS
JOURNAL OF THE AMERICAN CHEMICAL SOCIETY
Article
pubs.acs.org/JACS

Formal Reduction Potentials of Difluorotyrosine and Trifluorotyrosine Protein Residues: Defining the Thermodynamics of Multistep Radical Transfer

Kanchana R. Ravichandran,[†] Allan B. Zong,[§] Alexander T. Taguchi,[†] Daniel G. Nocera,[∥] JoAnne Stubbe,[†,‡] and Cecilia Tommos*[,§]

[†]Department of Chemistry and [‡]Department of Biology, Massachusetts Institute of Technology, 77 Massachusetts Avenue, Cambridge, Massachusetts 02139, United States

[§]Department of Biochemistry and Biophysics, University of Pennsylvania Perelman School of Medicine, Philadelphia, Pennsylvania 19104, United States

[∥]Department of Chemistry and Chemical Biology, Harvard University, 12 Oxford Street, Cambridge, Massachusetts 02138, United States

Supporting Information

ABSTRACT: Redox-active tyrosines (Ys) play essential roles in enzymes involved in primary metabolism including energy transduction and deoxynucleotide production catalyzed by ribonucleotide reductases (RNRs). Thermodynamic characterization of Ys in solution and in proteins remains a challenge due to the high reduction potentials involved and the reactive nature of the radical state. The structurally characterized α_3Y model protein has allowed the first determination of formal reduction potentials ($E^{o\prime}$) for a Y residing within a protein (Berry, B. W.; Martínez-Rivera, M. C.; Tommos, C. *Proc. Natl. Acad. Sci. U. S. A.* **2012**, *109*, 9739−9743). Using Schultz's technology, a series of fluorotyrosines (F_nY, n = 2 or 3) was site-specifically incorporated into α_3Y. The global protein properties of the resulting $\alpha_3(3,5)F_2Y$, $\alpha_3(2,3,5)F_3Y$, $\alpha_3(2,3)F_2Y$ and $\alpha_3(2,3,6)F_3Y$ variants are essentially identical to those of α_3Y. A protein film square-wave voltammetry approach was developed to successfully obtain reversible voltammograms and $E^{o\prime}$s of the very high-potential α_3F_nY proteins. $E^{o\prime}$(pH 5.5; α_3F_nY(O•/OH)) spans a range of 1040 ± 3 mV to 1200 ± 3 mV versus the normal hydrogen electrode. This is comparable to the potentials of the most oxidizing redox cofactors in nature. The F_nY analogues, and the ability to site-specifically incorporate them into any protein of interest, provide new tools for mechanistic studies on redox-active Ys in proteins and on functional and aberrant hole-transfer reactions in metallo-enzymes. The former application is illustrated here by using the determined α_3F_nY $\Delta E^{o\prime}$s to model the thermodynamics of radical-transfer reactions in F_nY-RNRs and to experimentally test and support the key prediction made.

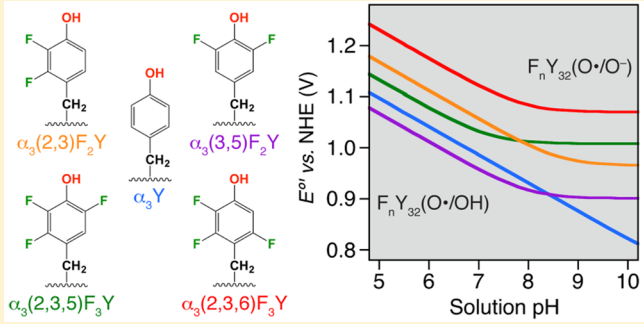

INTRODUCTION

The basic principles of electron tunneling (ET) in biological oxidation−reduction processes, within and between proteins, have been studied in great detail because of its centrality to so many important reactions.[1−3] These reactions usually involve metallo-prosthetic groups (e.g., hemes, iron−sulfur clusters, nonheme iron and copper cofactors) placed ∼14 Å apart within the protein environment. The rate constants for electron transfer (k_{ET}) depend on the electronic coupling of the electron donor and acceptor wave functions (H_{AD}), the energy required for the reorganization of their nuclear coordinates (λ), and the driving force (ΔG) for the reaction. k_{ET} is in general very fast and much faster than substrate redox chemistry (k_{cat}).

Also at the heart of biology are processes that involve the coupling of electron and proton movements, proton-coupled electron transfer (PCET).[4−8] These processes include among others, light-driven H_2O oxidation in oxygenic photosynthesis,[9] O_2 reduction in cellular respiration,[10] and deoxynucleotide synthesis required to make the building blocks for DNA replication and repair.[11] The basic principles of PCET reactions are actively being investigated and draw heavily on our understanding of ET. In PCET, however, the differences in mass between the electron and proton require much more constrained placement of the proton, typically between a H-bonded donor−acceptor pair, and minimization of charge build up in the low dielectric protein medium. The biological examples cited above all involve stable and/or transient tyrosyl radicals (Y−O•) as redox cofactors, which are the focus of this paper. Methods to study the involvement of these species have been limited since the biochemical systems typically have turnover numbers that are governed by conformational gating

Received: October 21, 2016
Published: February 7, 2017

DOI: 10.1021/jacs.6b11011
J. Am. Chem. Soc. 2017, 139, 2994−3004

(i.e., $k_{cat} \ll k_{PCET}$). Site-specific incorporation of unnatural amino acids (UAA) presents an approach to address this experimental barrier and disclose the underlying chemistry.[11−13] Recently, a tRNA/aminoacyl-tRNA synthetase (RS) pair was evolved to introduce 2,3,5-trifluorotyrosine into any protein of interest.[14] This RS turned out to be polyspecific and could incorporate both di- and trisubstituted fluorotyrosines (F_nY, n = 2, 3; Figure 1). These analogues are of interest for

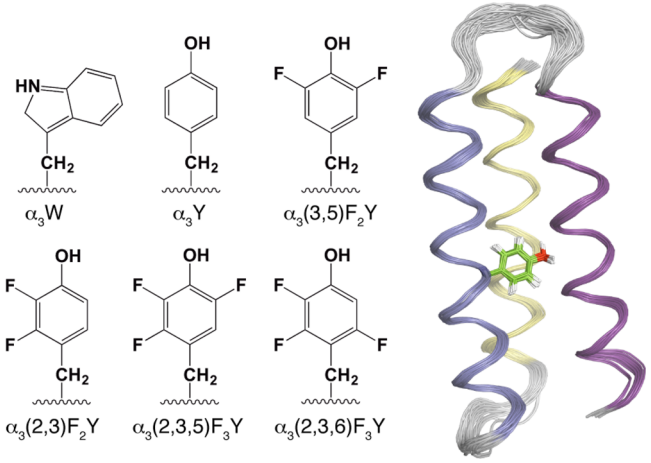

Figure 1. Six members of the α_3X family of de novo designed proteins. The 65-residue sequence common to these proteins: GSR(1)V KALEEKVKALEEKVKA−*LGGGGR*−IEELKKKX(32)EELKKKIEE−*LGGGGE*−VKKVEEEVKKLEEEIKK−L(65), forms a three-helix bundle (α_3) with an aromatic residue at a central position (site 32, labeled X).[25,26] The chemical structures display the side chain of residue 32 in α_3W, α_3Y and four α_3F_nY proteins. Solution NMR structures have been obtained for α_3W (PDB ID 1LQ7),[27] 2-mercaptophenol-α_3C (2MP-α_3C, 2LXY),[28] and α_3Y (2MI7; displayed as a ribbon diagram with the Y_{32} side chain in stick format).[29]

mechanistic studies of aromatic amino-acid PCET or "hole" hopping reactions since the ring substitutions alter the phenol pK_a and reduction potential significantly. Studies on the zwitterionic[15] and blocked forms (*N*-acetyl-F_n-L-tyrosinamides)[16] have shown that the pK_a is lowered from 10 for Y to the 6.4−7.8 range for the F_nYs. Anodic peak potentials (E_{peak}) obtained from irreversible voltammograms fall both below and above the corresponding E_{peak} of Y.[16] ΔE_{peak} spans ∼150 mV for the F_nY(O•/OH) redox pair and ∼165 mV for the F_nY(O•/O$^-$) couple. These variations offer the opportunity to perturb the biochemical systems such that individual PCET and chemical steps become experimentally accessible. This concept is illustrated by recent mechanistic studies on *E. coli* RNR.[17−20]

The broad utility of the F_nYs is also apparent from recent work on other biological systems. In studies on the photosystem II (PSII) reaction center, for example, 3-FY was globally incorporated to probe changes in the PCET kinetics of the active-site Y_Z residue using time-resolved absorption spectroscopy.[21] The active site of cytochrome *c* oxidase (C*c*O) also contains a redox-active Y species.[10] Lu and co-workers used a series of unnatural Y derivatives, including 3,5-F_2Y and 2,3,5-F_3Y, to study their influence on the reaction mechanism of a C*c*O model engineered into myoglobin.[22−24] Mechanistic studies revealed that pK_a values of Y and the Y analogues were correlated to O_2 reduction and H_2O production in this model system. Thus, F_nYs are emerging as an important tool to study radical-based protein PCET/hole hopping and to probe and alter active-site chemistry. An essential component currently missing with this approach is the knowledge of the formal reduction potentials ($E^{\circ\prime}$) of the F_nYs measured under reversible conditions and in a protein environment. The main reason the aqueous F_nYs give rise to irreversible voltammograms is because the Y−O• state is unstable on the time scale of the electrochemical measurements. Aqueous potentials reflect the thermodynamics of the redox-active species, but are also influenced by the kinetics of the Y−O• side reactions. Here we use the well-structured α_3X model protein system to stabilize the oxidized state of the F_nYs and render their electrochemical response reversible.

Position 32 is the dedicated radical site in the α_3X proteins (Figure 1).[25,26] This site is occupied by W_{32}, Y_{32}, $(3,5)F_2Y_{32}$,[30] or by a 2-, 3- or 4-mercaptophenol-C_{32} residue.[31] Nuclear magnetic resonance (NMR) and circular dichroism (CD) studies have shown that the α_3X proteins are highly helical, stable and well structured across a broad pH range.[25,29−32] Several of the α_3X proteins have been structurally characterized and residue 32 was confirmed to be solvent sequestered in each system.[27−29] The α_3 scaffold does not give rise to a Faradaic current in the absence of a redox-active residue at position 32.[28,31,32] Using square-wave voltammetry (SWV), Tommos and co-workers showed that Y_{32}, 2MP-C_{32} and $(3,5)F_2Y_{32}$ can be reversibly oxidized and reduced.[28,30,33] These studies demonstrate that pure thermodynamic potentials, uncompromised by Y−O• side reactions, can be obtained from the α_3X proteins. A photochemical study of α_3Y showed that Y_{32}−O• is formed in a PCET process and slowly ($t_{1/2}$ 2−10 s) decays via intermolecular radical−radical dimerization. The protein scaffold was shown to stabilize the Y_{32}−O• state by >10^4 relative to aqueous Y−O•.[29]

In this report we refine the SWV approach used in earlier α_3X studies to involve protein film voltammetry (PFV).[34] Protein film square-wave voltammograms were collected from α_3Y, $\alpha_3(3,5)F_2$Y, $\alpha_3(2,3)F_2$Y, $\alpha_3(2,3,5)F_3$Y and $\alpha_3(2,3,6)F_3$Y (Figure 1) at conditions where the global properties of the five proteins are close to identical. The obtained $E^{\circ\prime}$s of the α_3X proteins are compared to potentials reported for aqueous Y and F_nYs and for one of nature's most oxidizing redox cofactor. We find that, remarkably, the 7.5 kDa α_3X model protein can control a redox-active Y as oxidizing as the unique P_{680}^+/P_{680} redox pair, which drives the water-splitting process catalyzed by PSII. The α_3X potentials are also used to construct a thermodynamic model for RNR site-specifically labeled with the F_nYs shown in Figure 1. This model provides important insight into the first step in the multistep radical transfer (RT) process associated with nucleotide reduction in the class Ia RNRs.

MATERIALS AND METHODS

Protein Production and Spectroscopic Characterization. α_3Y was expressed and purified as described earlier.[29] 2,3,5-trifluorophenol was synthesized from 2,3,5-trifluorophenylboronic acid using a published protocol, with typical yields of ∼80%.[20,35] Tyrosine phenol lyase (TPL) was purified as previously reported.[36] All F_nYs (n = 2, 3) were enzymatically synthesized from the corresponding phenol using TPL as the catalyst following the published protocol.[37] SUMO protease was expressed from pTB145-*ulp1* as a His_6-tagged construct as previously reported.[38] Construction of the pE-SUMO-α_3TAG_{32} plasmid, optimization of the protein expression conditions, and the α_3F_nY protein purification protocol are described in the Supporting Information (SI). His_6-Y_{731}F-α2 was expressed and purified following

DOI: 10.1021/jacs.6b11011
J. Am. Chem. Soc. 2017, 139, 2994−3004

the published protocol for wild type (wt) α2.[14] 2,3-F_2Y_{122}•-β2 was expressed, purified and reconstituted as previously described.[18] Experimental conditions for all spectroscopic studies are described in detail in the SI.

PFV. SWV was performed using an Autolab PGSTAT12 potentiostat (Metrohm/Eco Chemie) equipped with a temperature-controlled, Faraday-cage protected three-electrode microcell (Princeton Applied Research). The Ag/AgCl reference electrode and the platinum wire counter electrode (Advanced Measurements Inc.) were prepared by filling the former with a 3 M KCl/saturated AgCl solution and the latter with 20 mM sodium acetate, 20 mM potassium phosphate, 20 mM sodium borate (APB) buffer containing 40 mM KCl. All measurements were carried out using a 3 mm diameter pyrolytic graphite edge (PGE) working electrode (Bio-Logic, USA). CD spectroscopy was used to determine the protein concentration in the α_3F_nY samples used to prepare the protein films. Samples were prepared by dissolving freeze-dried protein in buffer, measuring the 222 nm ellipticity (1 mm path) and calculating the protein concentration using the $[\Theta]_{222}$ values listed in Table S1. The final protein concentration was 45−80 μM. The electrode surface was prepared for protein adsorption by manually polishing its surface for 60 s in a 1.0 mm diamond/water slurry on a diamond polishing pad (Bio-Logic, USA) followed by 60 s in a 0.05 μm alumina/water slurry on a microcloth pad (Bioanalytical systems Inc.). The electrode surface was rinsed with methanol followed by an excess of milli-Q water (18 MΩ). The pH in the protein samples and in the electrolyte buffers were matched and measured prior to and after data collection. Solution resistance was compensated for by using the Autolab positive feed-back *iR* compensation function. Potentials are given versus the normal hydrogen electrode (NHE). Buffers and protein samples were prepared using ultra pure chemicals (Sigma-Aldrich) and data recorded under an argon atmosphere. Voltammograms were collected using the GPES software (Metrohm/Eco Chemie) and analyzed using PeakFit (Systat Software Inc.).

RESULTS

α_3F_nY Protein Expression and Purification. Construction and optimization (Figure S1) of the α_3F_nY protein expression system are described in the SI. The α_3F_nY yield was typically a few mg per L culture, except for $\alpha_3(2,3)F_2Y$ where it was significantly lower. Figure S2 shows analytical C18 chromatograms and MALDI-TOF traces of purified $\alpha_3(2,3)F_2Y$, $\alpha_3(2,3,5)F_3Y$ and $\alpha_3(2,3,6)F_3Y$. The protein preparations are homogeneous and display the correct α_3F_nY molecular weights. Equivalent data for purified $\alpha_3(3,5)F_2Y$ were presented in an earlier study.[30]

Protein Characterization. A key objective for the α_3X approach is to obtain a homogeneous set of $E^{\circ\prime}$(radical/amino acid) protein potentials, including the potentials for the F_nY_{32} residues. Practically this translates into: (i) determining the experimental conditions where the active redox couple is well-defined and the α_3 scaffold structurally unperturbed, and (ii) obtaining reversible protein voltammograms at these conditions. The phenol pK_a's of aqueous *N*-acetyl-F_n-L-tyrosinamides (n = 2, 3) range from 6.4 to 7.8.[16] α_3F_nY oxidation−reduction may thus involve Y_{32}(O•/OH), Y_{32}(O•/O^-) or a pH-weighted mixture of these two redox pairs. The UV−vis and CD studies described here were conducted to determine a common pH range where F_nY_{32}(O•/OH) is the dominant redox couple and the structural properties of the four α_3F_nYs (Figure 1) are minimally perturbed relative to α_3Y.

The apparent pK_a (pK_{app}) of X_{32} was determined to be 8.0 ± 0.1 for $\alpha_3(3,5)F_2Y$,[30] 7.2 ± 0.1 for $\alpha_3(2,3,5)F_3Y$ and 7.9 ± 0.1 for $\alpha_3(2,3,6)F_3Y$ (Figure 2; Table 1). The F_nY_{32} residues absorb poorly in the UV region[16] making the absorption-monitored pH titrations very material demanding. For $\alpha_3(2,3)F_2Y$, the amount of material precluded this measurement. The protein-induced increase in the phenol pK_a was very similar for $\alpha_3(3,5)F_2Y$, $\alpha_3(2,3,5)F_3Y$ and $\alpha_3(2,3,6)F_3Y$, with an average ΔpK_a of 0.83 ± 0.06 (Table 1). We assume that a shift of similar magnitude occurs for $\alpha_3(2,3)F_2Y$ and a pK_{app} of 8.6 (7.8 + 0.8) was predicted for this protein (Table 1).

CD spectroscopy was used to determine the α-helical contents and the global stabilities of the α_3F_nYs. Figure 3A compares the CD spectra of $\alpha_3(2,3)F_2Y$, $\alpha_3(2,3,5)F_3Y$ and $\alpha_3(2,3,6)F_3Y$ to the reference spectrum of α_3W at pH 5.05 ±

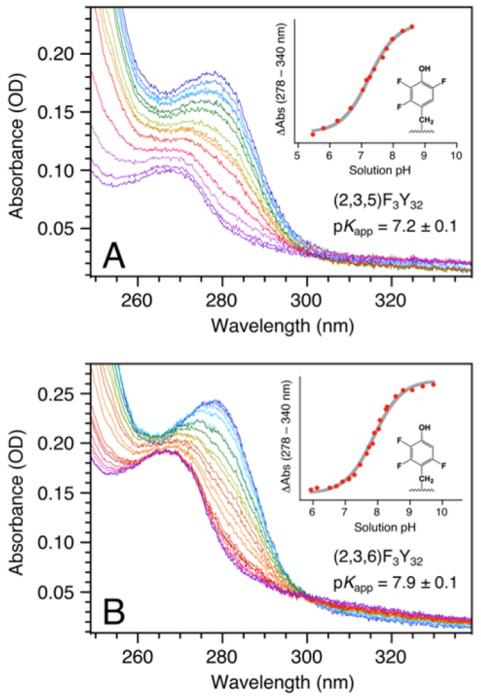

Figure 2. UV−vis spectra and corresponding pH-titration curves for (A) $\alpha_3(2,3,5)F_3Y$ and (B) $\alpha_3(2,3,6)F_3Y$. The $\alpha_3(2,3,5)F_3Y$ spectra were incrementally collected from pH 8.59 (dark blue) to pH 5.46 (dark purple) and back to pH 7.04 (red); while the $\alpha_3(2,3,6)F_3Y$ spectra were collected from pH 9.72 (dark blue)to pH 5.94 (dark purple) and back to pH 7.11 (red). The titration plots were fit to a single pK_a.

Table 1. pK_{app} and E_{net} Values for α_3Y and α_3F_nY (n = 2, 3)

system	pK_{app}	E_{net} (mV) (pH)[d]	ΔE_{net} (mV)[d]
$\alpha_3(3,5)F_2Y$	8.0[a]	1040 ± 3 (5.49 ± 0.03)	−25
α_3Y	11.3[b]	1065 ± 2 (5.53 ± 0.05)	0
$\alpha_3(2,3,5)F_3Y$	7.2	1104 ± 2 (5.54 ± 0.05)	+39
$\alpha_3(2,3)F_2Y$	8.6[c]	1136 ± 2 (5.57 ± 0.09)	+70
$\alpha_3(2,3,6)F_3Y$	7.9	1200 ± 3 (5.54 ± 0.05)	+135

system	pK_a[e]	DPV ΔE_{peak} (mV)[f]	CV ΔE (mV)[g]	
3,5-F_2Y	7.2	−51	−170[h]	
Y	10	0	0[h]	0[i]
2,3,5-F_3Y	6.4	+5	−122[h]	−107[i]
2,3-F_2Y	7.8	+44		− 40[i]
2,3,6-F_3Y	7.0	+97		

[a]Ref 30. [b]Ref 25. [c]Predicted value, see Results. [d]E_{net} = $E^{\circ\prime}$, see Discussion. [e]Aqueous *N*-acetyl-F_n-L-tyrosinamides. [f]For the Y(O•/OH) redox couple, Seyedsayamdost et al., ref 16. [g]Calculated for the Y(O•/OH) redox couple, see Discussion. [h]ΔE = anodic E_{peak} (F_nY − Y); Lu and co-workers, ref 23. [i]ΔE = electrode potential (F_nY − Y); Mahmoudi et al., ref 46.

DOI: 10.1021/jacs.6b11011
J. Am. Chem. Soc. 2017, 139, 2994−3004

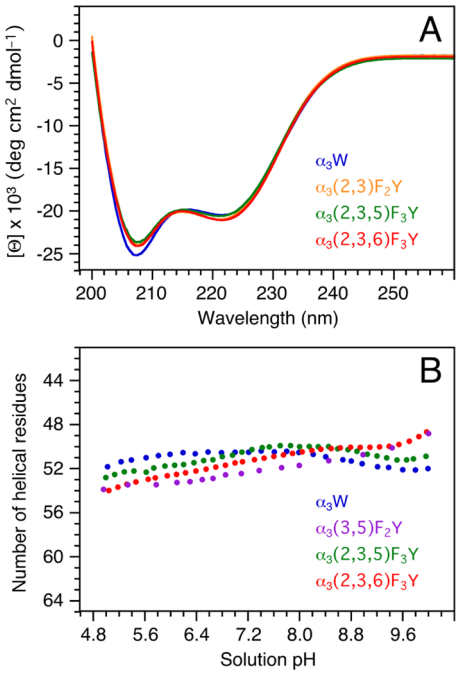

Figure 3. (A) Far-UV CD spectra of $\alpha_3(2,3,5)F_3Y$ (green), $\alpha_3(2,3)F_2Y$ (orange), $\alpha_3(2,3,6)F_3Y$ (red), and α_3W (blue; reference spectrum). The proteins were dissolved in 40 mM sodium acetate and the final sample pH measured to 5.05 ± 0.01. The spectra are displayed in units of mean residue molar ellipticity ($[\Theta]$) obtained by $[\Theta] = \theta_{obs}10^6/Cln$ where θ_{obs} is the observed ellipticity in millidegrees, C the protein concentration in μM, l the cuvette path length in mm (2), and n the number of amino-acid residues (65). C was determined using a fluorescence-based assay (SI). (B) pH-induced changes in the α-helical contents of $\alpha_3(3,5)F_2Y$ (purple; reproduced from ref 30), $\alpha_3(2,3,5)F_3Y$ (green), $\alpha_3(2,3,6)F_3Y$ (red) and α_3W (blue; reference data[25,27]).

0.01. The CD spectra are plotted in the normalized mean residue molar ellipticity form (see Figure 3 legend) where the 222 nm amplitude ($[\Theta]_{222}$) scales with the helical content. The spectra show that altering the Y_{32} ring has little impact on the helicity of the α_3 scaffold. The α-helical contents of $\alpha_3(2,3)F_2Y$, $\alpha_3(2,3,5)F_3Y$ and $\alpha_3(2,3,6)F_3Y$ were calculated from their CD spectra using the α_3W spectrum as the reference. $[\Theta]_{222}$ values and corresponding α-helical contents are listed in Table S1.

Figure 3B displays changes in the total number of α-helical residues in $\alpha_3(3,5)F_2Y$,[30] $\alpha_3(2,3,5)F_3Y$ and $\alpha_3(2,3,6)F_3Y$ as a function of pH. A pH plot of α_3W is also shown (51 ± 0.6 α-helical residues, pH 4−10).[25,27] The pH-induced structural changes are minor and the α_3F_nYs have the same or somewhat higher α-helical content than α_3W below pH 6.8. The global stabilities of $\alpha_3(2,3,5)F_3Y$ and $\alpha_3(2,3,6)F_3Y$ were determined by urea denaturation at pH 5.0 and 5.5. Representative data are shown in Figure S3 and protein stability values for α_3Y,[29,32] $\alpha_3(3,5)F_2Y$,[30] $\alpha_3(2,3,5)F_3Y$ and $\alpha_3(2,3,6)F_3Y$ are summarized in Table S1. For the pH 5.0−5.5 range, there is no significant difference in the global stability of α_3Y, $\alpha_3(3,5)F_2Y$ and $\alpha_3(2,3,5)F_3Y$ while $\alpha_3(2,3,6)F_3Y$ is 0.4 kcal mol^{-1} more stable than α_3Y. The minimal variations in α-helical content and global stabilities of the α_3F_nYs relative to α_3Y are in accordance with previous observations in other proteins.[39] Fluorination of amino acids has been shown to result in minimal structural perturbations to the global protein fold.[40,41] Additionally, the increased hydrophobicity resulting from fluorination usually enhances protein stability.[39,42,43]

We conclude that the common pH range sought for the α_3F_nY voltammetry studies is limited by the pK_{app} of $\alpha_3(2,3,5)F_3Y$ (7.2; to drive the system toward $Y_{32}(O\bullet/OH)$) rather than by considerations of the structurally robust α_3 scaffold.

Protein Film Square-Wave Voltammetry on the α_3F_nY Proteins. SWV is a pulse voltammetric technique supported by well-developed theoretical models for diffusion-controlled and surface-confined electrode mechanisms.[44,45] SWV was used to obtain formal $E^{o\prime}$(radical/amino acid) protein potentials for α_3Y,[33] 2MP-α_3C,[28] and $\alpha_3(3,5)F_2Y$.[30] The α_3X potentials are pH dependent and measurements performed at low pH are more difficult due to the higher potentials and more pronounced background currents involved.[33] SWV on $\alpha_3(2,3,5)F_3Y$, $\alpha_3(2,3)F_2Y$, and $\alpha_3(2,3,6)F_3Y$ was predicted to be challenging since measurements had to be done ~pH 5.5 (≥1.7 pH units below the pK_{app}'s of the α_3F_nY proteins) and test studies on $\alpha_3(2,3,5)F_3Y$ placed $E^{o\prime}$ well above +1 V. Voltammetry data from an ongoing parallel project involving an $\alpha_3(NH_2)Y$ variant (Lee, Nocera, Stubbe and Tommos) suggested that a protein film approach, where the protein is introduced to the surface of the working electrode outside the electrochemical cell, improves the Faradaic response of the α_3X system. A protein film protocol was developed for α_3Y and applied to the α_3F_nY proteins. This approach allowed us to obtain high-quality reversible voltammograms in a potential range unprecedented for protein voltammetry and to determine the formal potentials of the highly oxidizing α_3F_nYs.

In SWV the applied potential is stepped progressively in fixed increments (E_{step}), and at each increment, a forward (here oxidative) potential pulse is applied followed by a reverse (reductive) pulse. The current is sampled at the end of each alternating pulse and plotted as a function of E_{step}. This generates a forward (I_{for}), a reverse (I_{rev}) and a net ($I_{net} = I_{for} - I_{rev}$) voltammogram. The time period (τ) over which the electrode reaction is driven in the anodic and then cathodic direction is set by the SW frequency ($f = 1/\tau$).[44,45] The apparent redox reversibility of a surface-adsorbed redox pair is described by a kinetic parameter (ω) defined as the ratio of the surface standard ET rate constant (k_{sur}) and the SW frequency ($\omega = k_{sur}/f$). Theory predicts that the strongest response from an adsorbed redox pair occurs when f is close to k_{sur}.[47] In earlier reports, the Faradaic response of α_3Y and 2MP-α_3C were investigated over a broad frequency range of 30−960 Hz and 30−720 Hz, respectively.[28,33] Figure S4 shows I_{net} of α_3Y (blue) and 2MP-α_3C (red) divided by f, and the obtained I_{net}/f amplitudes plotted against the frequency. The parabolic shape of the frequency-normalized data is consistent with the "quasi-reversible maximum" (QRM) feature of surface-confined redox reactions.[47] The α_3Y and 2MP-α_3C plots are almost identical with a QRM at 440 Hz. The α_3F_nYs were anticipated to behave in a similar fashion and display the strongest Faradaic response around 440 Hz. Test studies on $\alpha_3(2,3,5)F_3Y$ confirmed that the most pronounced response was observed in a rather narrow frequency range of ~400 to 450 Hz. The response was poor above and below this range (data not shown). SWV on the α_3F_nY proteins was thus conducted using a SW frequency of 440 Hz.

Background-corrected protein film SW voltammograms of α_3Y are displayed in Figure 4A. The forward, reverse and net currents are colored orange, purple and blue, respectively. The measurement was performed as follows: The surface of the PGE working electrode was polished (see Materials and

DOI: 10.1021/jacs.6b11011
J. Am. Chem. Soc. 2017, 139, 2994−3004

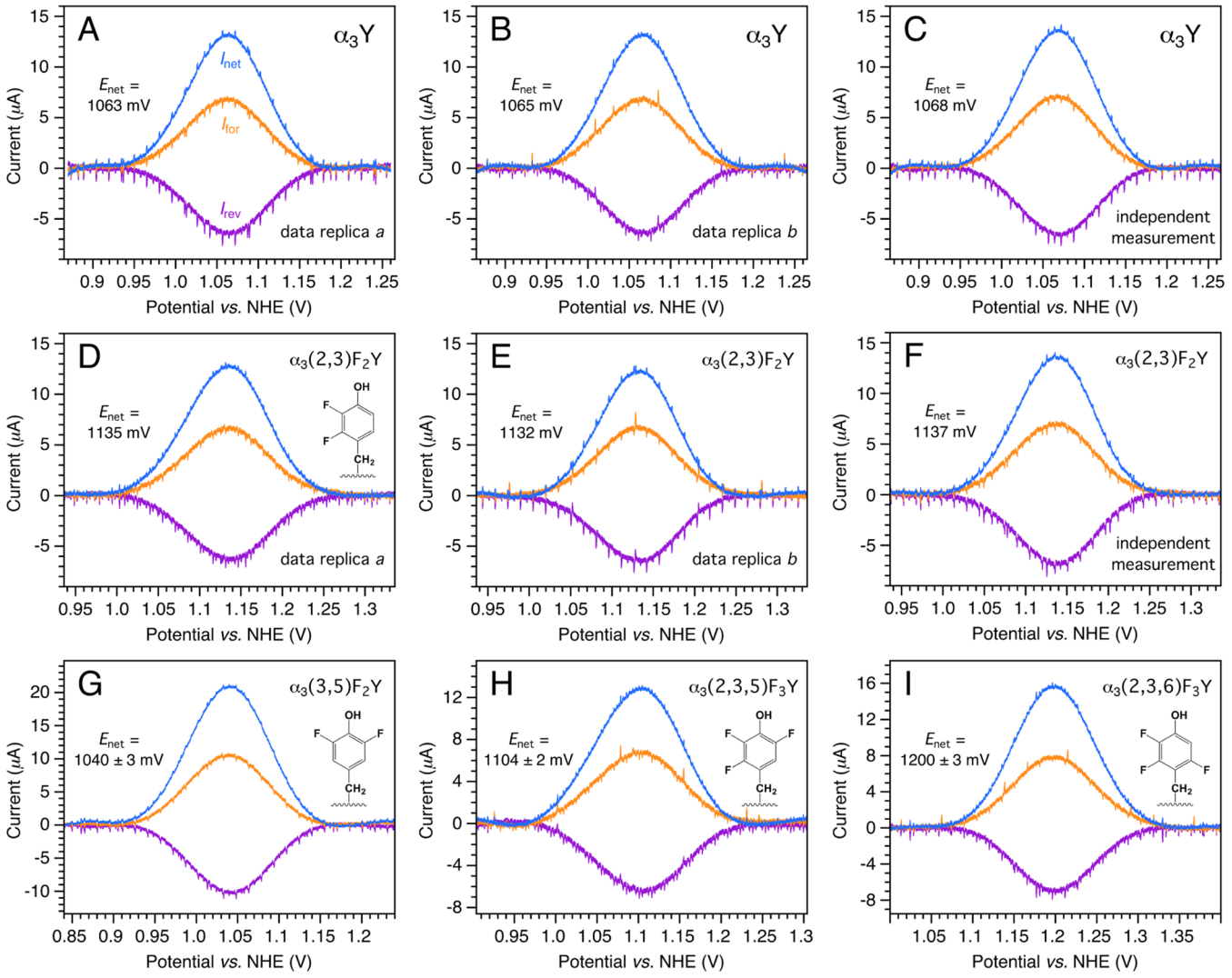

Figure 4. Background-corrected protein film SW voltammograms of (A–C) α_3Y, (D–F) $\alpha_3(2,3)F_2$Y, (G) $\alpha_3(3,5)F_2$Y, (H) $\alpha_3(2,3,5)F_3$Y, and (I) $\alpha_3(2,3,6)F_3$Y. The proteins were adsorbed onto the surface of a PGE electrode and voltammograms recorded in 20 mM APB, 40 mM KCl, pH 5.54 ± 0.06 buffer at 25 °C. SWV settings: Equilibration time 5 s, step potential 0.15 mV, SW pulse amplitude 25 mV, SW frequency 440 Hz.

Methods for details) and introduced to a 500 μL 80 μM α_3Y, 20 mM APB, 75 mM KCl, pH 5.5 sample for 30 s. The electrode was transferred to a blank electrochemical cell containing 3 mL 20 mM APB, 40 mM KCl, pH 5.5 and a voltammogram recorded. This procedure was repeated twice to collect data replicas *a* and *b* (data panels A and B) and on a separate experimental day using an independently prepared protein sample (panel C). The maximum amplitude of I_{net} was investigated as a function of the electrode surface/α_3Y sample incubation time and found stable after about 20 s. No increase in I_{net} was observed at incubation times >30 s.

The protein film protocol described above was applied to $\alpha_3(2,3)F_2$Y and the resulting voltammograms are displayed in the middle row of Figure 4. The corresponding uncorrected data for the baseline-subtracted α_3Y (Figures 4A–C) and $\alpha_3(2,3)F_2$Y (Figures 4D–F) voltammograms are shown in Figures S5 and S6, respectively. Data processing and analysis details are provided in the SI. As shown in Figures 4, S5 and S6, the voltammograms are recorded at very high positive potentials and the background currents are significant. Nonetheless, the I_{for}, I_{rev} and I_{net} waveforms are well-defined and their position, line shape and amplitude are highly reproducible between data replicas and independent measurements. Representative protein film voltammograms collected from $\alpha_3(3,5)F_2$Y, $\alpha_3(2,3,5)F_3$Y and $\alpha_3(2,3,6)F_3$Y are shown in Figure 4 panels G, H, and I, respectively. The pH in the protein samples and in the electrolyte solutions were measured at the beginning and at the end of each experimental day. The average pH, E_{net} and ΔE_{net} values are listed in Table 1.

Summarizing the Redox Properties of the α_3F_nY Proteins as E_{net} vs pH Diagrams. A set of E_{net} vs pH diagrams was predicted for the α_3F_nYs based on the results described above combined with the established charge-neutral response of the α_3X redox system.[28,31,33] The plots shown in Figure 5 were constructed from the following data: (i) The four α_3F_nY E_{net} pH 5.5 values listed in Table 1 (single dots colored purple, green, orange and red). (ii) The α_3Y E_{net} pH 5.53 ± 0.05 value listed in Table 1 plus three additional PFV E_{net} values obtained at pH 6.94 ± 0.07, 8.40 ± 0.10 and 9.94 ± 0.08 (blue dots; Figure S7). The pH dependence (55.2 mV/pH unit) of the Y_{32}(O•/OH) potential is consistent with an overall charge-neutral redox cycle where the 1e$^-$ oxidation–reduction process driven by the electrode is coupled to the release/uptake of essentially one full H$^+$ to/from bulk.[33] (iii) $\alpha_3(3,5)F_2$Y E_{net}

DOI: 10.1021/jacs.6b11011
J. Am. Chem. Soc. 2017, 139, 2994–3004

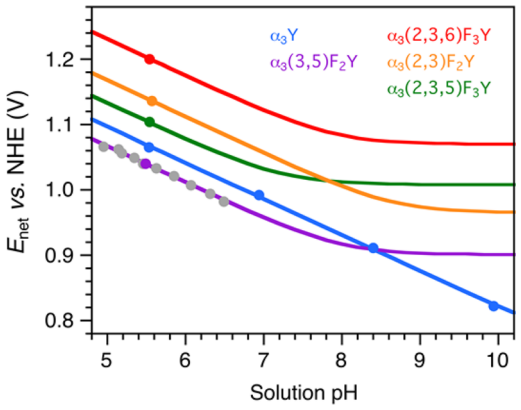

Figure 5. E_{net} vs pH diagrams for α_3Y and the α_3F_nY proteins. Solid dots represent E_{net} values obtained by PFV. Gray dots represent E_{net} collected from $\alpha_3(3,5)F_2Y$ using the following conditions: 70 μM protein, 20 mM APB, 75 mM KCl; pH adjusted with 1 M NaOH; step potential 0.15 mV, SW pulse amplitude 25 mV, SW frequency 190 Hz, and temperature 25 °C.

measured between pH 4.95 ± 0.01 and 6.49 ± 0.02 (gray dots). The pH titration was done on $\alpha_3(3,5)F_2Y$ since it has a higher pK_{app} than $\alpha_3(2,3,5)F_3Y$ and $\alpha_3(2,3,6)F_3Y$, and expresses better than $\alpha_3(2,3)F_2Y$. Additionally, the potential is lower than for the other α_3F_nYs making the measurements less challenging. The pH titration was done with $\alpha_3(3,5)F_2Y$ in the electrochemical cell (details provided in the Figure 5 legend). The pH dependence in E_{net} (55.7 mV/pH unit) was used to predict the E_{net} vs pH curves for all of the α_3F_nYs. (iv) The pK_{app}'s of $\alpha_3(3,5)F_2Y$, $\alpha_3(2,3,5)F_3Y$ and $\alpha_3(2,3,6)F_3Y$ and (v) the predicted pK_{app} of $\alpha_3(2,3)F_2Y$ (Table 1). The Nernst equations and parameters used to model the diagrams are listed in Table S2. Table S2 also lists the α_3F_nY potentials at pH 7.0 as a general reference.

DISCUSSION

The α_3X System Combined with Protein Film SWV Facilitates Studies of "Hot" Radicals. The experimental advance made here was driven by the very "hot" nature of the F_nY_{32} radicals and the necessity of recording reversible voltammograms at exceedingly high potentials. This issue was addressed by employing PFV.[34]

Voltammograms collected at high positive potentials contain capacitive currents, background currents from the oxidation of the solvent, supporting electrolytes and/or chemical groups on the surface of the working electrode (WE), in addition to the Faradaic current of the redox-active species under investigation. The effects of capacitive currents can be minimized by using pulse voltammetric techniques, such as differential pulse voltammetry (DPV) or SWV. Background currents from solvent oxidation can be reduced by using a carbon, rather than a metal-based, WE but they cannot be eliminated. Prominent background currents are unavoidable when doing high-potential voltammetry on aqueous systems and they rapidly increase above ~1 V. Thus, an increase in $E^{\circ\prime}$ that would be insignificant when probing a 0.5 V protein oxidant may prove challenging, even prohibiting, when probing a protein oxidant in the +1.0 V range. Berry et al. used SWV and a PGE electrode to optimize the α_3Y response and showed that Y_{32} can be reversibly oxidized and reduced.[33] Here we show that the α_3Y response improves even further when the protein is adsorbed onto the surface of the PGE electrode outside the electrochemical cell. The protein film samples gave rise to Faradaic currents that are easily identified above the background (Figures S5 and S6). Baseline-corrected traces with well-defined peak positions and lineshapes were reproducibly obtained despite the high potentials involved (Figure 4; Table 1). The protein film SW voltammograms collected from α_3Y and the α_3F_nYs display an I_{for}/I_{rev} close or equal to unity and an $E_{for} - E_{rev}$ peak separation of −2 ± 2 mV. This is consistent with a strongly adsorbed redox pair for which the surface standard ET rate constant k_{sur} is close to the SW frequency (f = 440 s^{-1}) and E_{net} equals $E^{\circ\prime}$.[48]

The α_3X Potentials Reflect the Local Protein Environment. Previous DPV and SWV studies were conducted with the α_3X proteins dissolved in the supporting electrolyte solution.[28,30−33] The characteristics of their Faradaic response suggested that diffusion-controlled reactions dominated the electrode process.[28,33] As described above, the I_{net} amplitude stabilizes in less than 20 s of exposing the surface of the PGE electrode to an α_3Y sample. Data collected with the protein dissolved in the electrolyte solution would typically be started on this time scale after the freshly polished WE was placed in the cell. Previously published α_3X voltammograms thus most likely represent a mixed contribution of surface-adsorbed and diffusional species.

Figure 5 shows a α_3Y E_{net} vs pH diagram constructed from PFV data. All previously reported α_3Y potentials recorded over a broad range of conditions (method, SWV or DPV; WE material, pyrolytic graphite or glassy carbon; [protein] 2−210 μM; [KCl] 10−140 mM; pH 5.5−10; SW frequency 190−960 Hz)[33] were plotted against values predicted from the α_3Y PFV E_{net} vs pH diagram in Figure 5. The plot goes through zero and displays a linear correlation of 1.001 ± 0.002 and a standard error of < ±7 mV (not shown). Thus, there is no significant change in the observed potential when the system shifts from mixed surface/diffusional to a pure surface mechanism. This is also true for $\alpha_3(3,5)F_2Y$ (E_{net}(pH 5.70) 1026 ± 4 mV in ref 30 and 1028 ± 3 mV in Figure 5). These observation are consistent with the buried position of Y_{32}[29] where the Y_{32}(O•/OH) potential is only influenced by local protein interactions and not by external factors such as charges on the surface of the WE.

Interestingly, there is a symmetry to the α_3F_nY $\Delta E^{\circ\prime}$s (Table 1). When the common component (2-FY = 6-FY, i.e., F attached to either of the two ring delta carbons) is isolated by pairing the four independently obtained $E^{\circ\prime}$s, the same value is obtained:

$$\alpha_3(2,3,5)F_3Y(1104\text{ mV}) - \alpha_3(3,5)F_2Y(1040\text{ mV}) = 64\text{ mV}$$

$$\alpha_3(2,3,6)F_3Y(1200\text{ mV}) - \alpha_3(2,3)F_2Y(1136\text{ mV}) = 64\text{ mV}$$

We interpret this to show that the impact of the local protein environment on the F_nY_{32}(O•/OH) $E^{\circ\prime}$s is equal across the four proteins. If the asymmetrically labeled F_nY_{32} side chains have multiple rotameric states,[18,49] it has little influence on their $E^{\circ\prime}$s.

***E*°′(Y(O•/OH)) Increases by about 45−65 mV When Placed in a Hydrophobic Protein Environment.** Zwitterionic and blocked Y have been studied by pulse radiolysis,[50−52] cyclic voltammetry (CV),[23,46,53,54] DPV[25,54,55] and SWV.[46] The reported pH 7.0 potentials span a considerable range, 830−970

DOI: 10.1021/jacs.6b11011
J. Am. Chem. Soc. 2017, 139, 2994−3004

mV, which reflects a number of issues. In pulse radiolysis, equilibrium is established between a reference redox couple and the redox couple of interest. For accurate readings, equilibrium must be established on a time scale that is fast relative to Y–O• decay. Additionally, some of the reference potentials used in the older literature were not as well-determined as they are today.[56] Aqueous Y gives rise to irreversible voltammograms since Y–O• dimerization is fast (k_{dim} 2–7 × 10^8 M^{-1} s^{-1})[29,57] relative to the experimental time scale. These voltammograms, which display only an anodic wave, may reflect a reversible, quasi-reversible or irreversible electrode reaction. If the electrode reaction is shown to be reversible,[58] then the anodic peak potential can be corrected for k_{dim} and an apparent formal potential derived.[58,59] Harriman[53] and DeFelippis et al.[54] applied this approach but unfortunately used an incorrect equation to compensate for k_{dim}.[46] Recently reported (or recommended) pH 7.0 potentials for aqueous Y are 0.93 ± 0.02 V,[52] 0.91 ± 0.02 V,[56] and 0.96 V.[46] We therefore take a consensus value of 920–940 ± 20 mV for the aqueous Y(O•/OH) redox couple at pH 7.0. $E^{\circ\prime}$ of Y_{32}(O•/OH) is 986 ± 3 mV at pH 7.0 (Figure 5; Table S2). Thus, the potential of the Y(O•/OH) couple increases by ~45–65 ± 20 mV when Y is buried inside α_3Y.

Comparing F_nY Potentials Obtained at Reversible and Irreversible Conditions. Tommos et al.[25] and the Stubbe and Nocera groups[11,16,55] have reported raw DPV potentials for Y, W and Y analogues. The focus of these studies was to obtain comparable peak potentials for Y vs W,[25] Y vs NO_2Y,[55] and Y vs F_nYs.[16] Tommos and collaborators are using the unique α_3X system to refine and solidify these ΔEs by comparing the true thermodynamic E°'s of Y_{32},[33] W_{32} (Tommos, Hammarström, in preparation), NO_2Y_{32} (Tommos, ongoing) and F_nY_{32} (this study). Table 1 displays absolute and relative E°'s for α_3Y and the α_3F_nYs proteins and compares the latter to ΔE_{peak} values obtained by DPV. The absolute potentials differ by ~168 mV (α_3Y − Y)[25,55] and ~193 mV (α_3F_nY − F_nY).[16] These differences reflect the water vs protein medium (~45–65 ± 20 mV, vide supra), a DPV pulse amplitude factor (25 mV), and peak shifts due to the irreversibility of the aqueous systems (~90 ± 10 mV for Y and ~115 ± 10 mV for the F_nYs). Nonetheless, the relative potentials reported in ref 16 fit rather well with the α_3X data. The oxidizing power of the Ys increases in the same order (3,5-F_2Y < Y < 2,3,5-F_3Y < 2,3-F_2Y < 2,3,6-F_3Y) and the overall span (E(2,3,6-F_3Y) − E(3,5-F_2Y)) is 160 mV and ~150 mV for the α_3F_nYs and F_nYs, respectively. One significant difference between the α_3X Δ$E^{\circ\prime}$ scale and the DPV ΔE_{peak} scale in Table 1 is that the four E_{peak}(F_nY)s are downshifted by ~30 mV relative to E_{peak}(Y). This does not represent a true difference in potential between the protein and aqueous systems but rather reflects the limitations of relying on irreversible voltammograms. Recently, Lu and co-workers[22,23] and Mahmoudi et al.[46] used CV to measure the differences in anodic peak (or electrode) potentials derived from irreversible voltammograms of aqueous 3,5-F_2Y, 2,3,5-F_3Y and 2,3-F_2Y relative to Y. Overall, there is little consensus in the values reported for the aqueous systems with ΔE(pH 7.0; 3,5-F_2Y − Y) ranging from −158 to −60 mV[11,23] ΔE(pH 7.0; 2,3,5-F_2Y − Y) from −81 to +30 mV,[11,23,46] and ΔE(pH 7.0; 2,3-F_2Y − Y) from −30 to +30 mV.[11,46] Table 1 lists CV ΔE values for the Y(O•/OH) redox couple (i.e., at 2 pH units below the phenol pK_a's) as calculated from the reported pH 7.0 values.[23,46] This representation allows for a direct comparison to the α_3X(O•/OH) ΔE°'s. The large discrepancies observed for the aqueous ΔE values highlight the importance of measuring the potentials of reactive radicals under reversible conditions such as those achieved here.

Using the a_3X System to Model the Initial RT Step in F_nY_{122}•-β2: PCET or ET? Below we explore the general use of the α_3X potentials by applying them as an analytical tool to investigate RT in *E. coli* RNR. This enzyme consists of two homodimeric subunits, α2 and β2, which form the active $\alpha2\beta2$ complex.[11] β2 contains a stable diferric-Y_{122}• cofactor that reversibly generates a transient thiyl radical in α2 (C_{439}•; Figure 6). Once formed, C_{439}• initiates the catalytic nucleotide

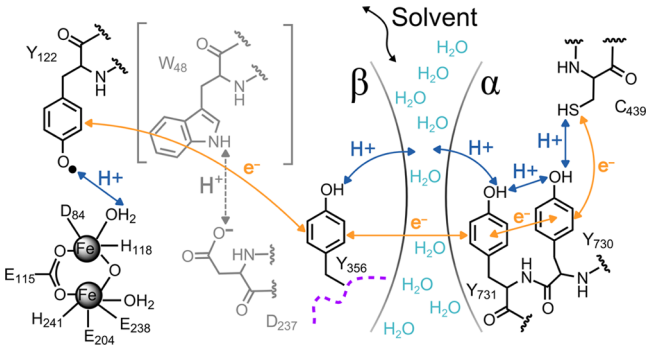

Figure 6. Radical transfer pathway in *E. coli* RNR. The arrows represent electron (orange) and proton (blue) movements within the α2 and β2 subunits. There is currently no evidence for the involvement W_{48} (gray) or its proposed proton acceptor D_{237} (gray) in RT. The $\alpha2/\beta2$ water interface is suggested in refs 60 and 63.

reduction process. Each turnover involves multistep RT via Y_{122}–O• ⇆ [W_{48}?] ⇆ Y_{356} in β2 and Y_{731} ⇆ Y_{730} ⇆ C_{439} in α2 (Figure 6). Slower conformational gating masks the forward and reverse RT steps and the transient Y_{356}•, Y_{730}• and Y_{731}• species are not observed in wt RNR. Site-specific incorporation of NO_2Y and F_nY residues proved to be a successful approach to perturb the system so that the pathway Y radicals can be observed.[11,61,62] The following ΔE°'s were obtained from the radical distribution patterns at equilibrium: Δ$E^{\circ\prime}$(pH 7.6; 2,3,5-F_3Y_{122}• − Y_{356}•) = 20 ± 10 mV, Δ$E^{\circ\prime}$(pH 8.2; Y_{122}• − 3,5-F_2Y_{356}•) = −70 ± 5 mV, and Δ$E^{\circ\prime}$(pH 7.6; Y_{356}• − Y_{731}•) = ~ −100 mV at 25 °C.[62,63] Taken together these ΔE°'s sketch out the thermodynamic landscape associated with the intersubunit RT pathway in *E. coli* RNR (Figure S8).[63]

In the analysis presented below, we combine the α_3X potentials with two of the RNR ΔE°'s listed above to construct a thermodynamic model for sites Y_{122} and Y_{356} in wt and F_nY-RNRs. The modeling addresses the question if the initial RT step in 2,3,5-F_3Y_{122}•-β2 is PCET (established for wt RNR; Figure 7A)[64] or ET (established for NO_2Y_{122}•-β2: Figure 7B)[61] and if this process is identical between the different F_nY_{122}•-β2 systems.

Modeling of RNR Sites 356 and 122. Figure 8 displays a thermodynamic model for sites 356-β2 (Panel A) and 122-β2 (Panel B) in wt and F_nY-RNRs. The Y_{356} site was modeled by using the absolute α_3X potentials (Figure 5) and phenol pK_a's that were upshifted by 0.4 relative to the aqueous F_nYs (Figure 8A). The modeled potentials are pH dependent since the proton released upon Y_{356} oxidation is in rapid exchange with the bulk solvent.[63] The pK_a values are based on the 0.4 increase in the pK_a of NO_2Y_{356}.[65] The modeling of site 122 was more involved and is described in a stepwise manner below and in Figure 8B.

DOI: 10.1021/jacs.6b11011
J. Am. Chem. Soc. 2017, 139, 2994–3004

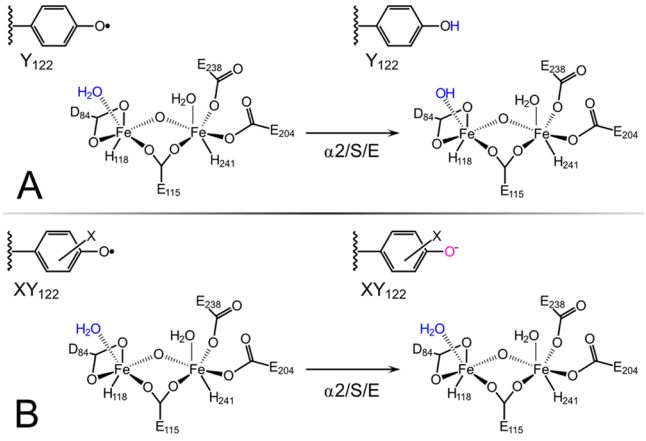

Figure 7. Initiation of RT when (A) wt-β2 or (B) XY-β2 (where X is NO_2 or F_n) reacts with α2, substrate CDP (S) and allosteric effector ATP (E). (A) Reduction of wt Y_{122}–O• by Y_{356} is coupled with proton transfer (PT) from Fe1–H_2O.[64] (B) Reduction of NO_2Y_{122}–O• (or F_nY_{122}–O•) by Y_{356} is not coupled to PT from the diiron cluster.

In wt RNR, Y_{122}(O•/OH) is the active redox couple and the proton toggles between the phenol oxygen and the Fe1(H_2O/OH) species (Figure 7A).[64] The site is effectively not in communication with bulk and is therefore modeled with pH-independent potentials. The Y_{356} (blue) and 3,5-F_2Y_{356} (purple) $E^{\circ\prime}$ vs pH diagrams displayed in Figure 8A are reproduced in Figure 8B. By combining these Y_{356} plots with the RNR ΔE°'s obtained in ref 63 (illustrated by black arrows), the potentials of sites 356 and 122 were linked as follows: The potential of 2,3,5-F_3Y_{122} was obtained by taking the predicted $E^{\circ\prime}$(Y_{356}(O•/OH)) pH 7.6 value (953 mV, blue dot) and making $E^{\circ\prime}$(2,3,5-F_3Y_{122}) 20 ± 10 mV more oxidizing (973 mV; green line). Likewise, the potential of Y_{122}(O•/OH) was obtained by taking the predicted $E^{\circ\prime}$(3,5-F_2Y_{356}) pH 8.2 value (928 mV, purple dot) and making $E^{\circ\prime}$(Y_{122}(O•/OH)) 70 ± 5 mV less oxidizing (858 mV; black line). Importantly, this model predicts a +95 mV uphill step between wt Y_{122} and Y_{356} (at pH 7.6 and 25 °C; red double arrow).

The α_3X $\Delta E^{\circ\prime}$(pH 5.5) scale in Table 1 mainly reflects changes in the Y_{32} fluorination pattern since the other key properties of the redox system (overall charge neutral redox cycle; buried hydrophobic site) are the same between α_3Y and the α_3F_nYs. This situation suggests that the α_3X ΔE°'s can be used as a diagnostic tool. A RNR $\Delta E^{\circ\prime}$ that deviates significantly from the corresponding α_3X $\Delta E^{\circ\prime}$ is an indicator that some property, in addition to the Y fluorination pattern, has changed. Table 1 predicts a 39 mV difference ($\Delta E^{\circ\prime}$(α_3(2,3,5)F_3Y − α_3Y)) between Y_{122}(O•/OH) (black) and 2,3,5-F_3Y_{122}(O•/OH) (gray dotted line). This is not consistent with the 115 mV difference between Y_{122}(O•/OH) and 2,3,5-F_2Y_{122} obtained in step 1 above (black and green lines). Below we examine the possibility that the initial RT step has changed from PCET in wt RNR to ET in 2,3,5-F_3Y_{122}-β2.

Y(O•/O^-) is the experimentally observed redox pair in the single turnover (NO_2)Y_{122}-β2 system.[61] It appears likely that Y(O•/O^-) is the active redox couple also in 2,3,5-F_3Y_{122}-β2 since the pK_a of 2,3,5-F_3Y (6.4)[16] is lower than the pK_a of NO_2Y (7.1).[55] In this scenario, oxidation–reduction of native Y_{122} involves ET between Y_{356} and Y_{122}, PT between Fe1(H_2O/OH) and Y_{122}(O•/OH), and a net charge change at the diiron cluster (Figure 7A). In contrast, oxidation–reduction of 2,3,5-F_3Y_{122}-β2 involves ET between Y_{356} and Y_{122} and a net charge change at site 122 (Figure 7B). The 115 mV difference in potential between Y_{122}(O•/OH) and 2,3,5F_3Y_{122}(O•/O^-) is partly due to the ring fluorination and partly due to redox-driven electrostatic changes that are not identical between the wt system and 2,3,5-F_2Y_{122}-β2.

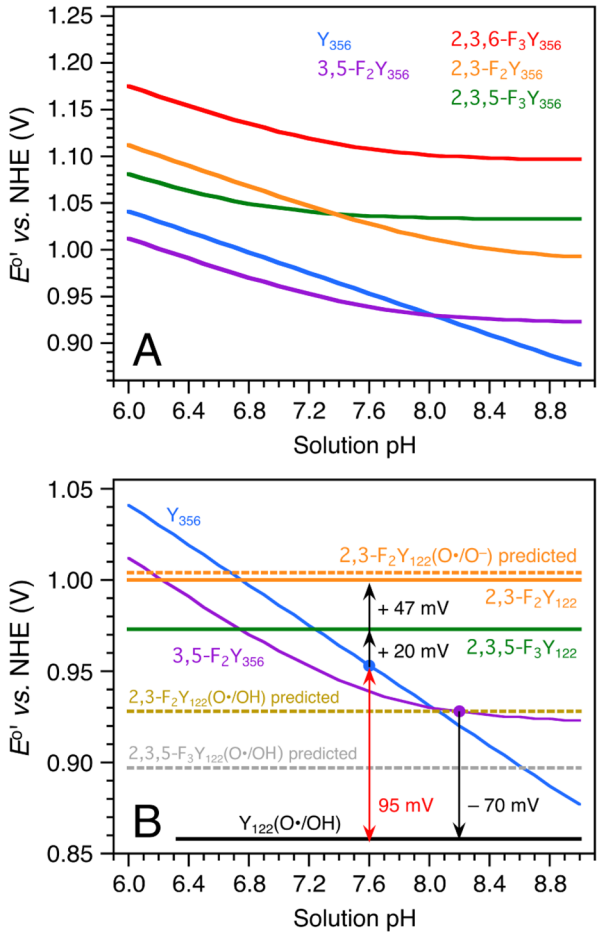

Figure 8. Thermodynamic model for sites Y_{122} and Y_{356} in wt and F_nY-RNR. (A) Predicted $E^{\circ\prime}$ vs pH diagrams for residue Y_{356} in the wt RNR and in mutants containing F_nY_{356} (n = 2, 3) residues. Y_{356} is modeled with a pK_a of 10.4, which makes Y_{356}(O•/OH) the dominant redox couple across the displayed pH range. The F_nY_{356} residues are modeled with lower pK_a's (3,5-F_2 7.6; 2,3,5-F_3 6.8; 2,3-F_2 8.2; 2,3,6-F_3 7.4) and their potentials are described by a pH-weighted mixture of the F_nY_{356}(O•/OH) and F_nY_{356}(O•/O^-) redox pairs. (B) Modeled E°'s for residue Y_{122} in the wt and F_nY_{122}-RNRs. The Y_{356} (blue) and 3,5-F_2Y_{356} (purple) $E^{\circ\prime}$ vs pH diagrams are superimposed from Panel A. The black arrows represent experimentally obtained ΔE°'s (Figures S8 and S9).[63] A +95 mV step is predicted for RT from Y_{122}(O•/OH) to Y_{356} (O•/OH) in wt RNR (red double arrow). The E°'s are modeled for 25 °C.

2,3-F_2Y has a higher pK_a (7.8) than the other F_nYs (6.4–7.2) and 2,3-F_2Y_{122} may thus behave as Y_{122}(O•/OH) or as 2,3,5-F_3Y_{122}(O•/O^-). If it is the former, we predict a $\Delta E^{\circ\prime}$ of 70 mV ($\Delta E^{\circ\prime}$(α_3(2,3)F_2Y − α_3Y); Table 1) between Y_{122}(O•/OH) and 2,3-F_2Y_{122}(O/OH) (928 mV; tan dotted line). If it is the latter, we predict a $\Delta E^{\circ\prime}$ of 31 mV ($\Delta E^{\circ\prime}$(α_3(2,3)F_2Y − α_3(2,3,5)F_3Y); Table 1) between 2,3,5-F_3Y_{122}(O•/O^-) and 2,3-F_2Y_{122}(O•/O^-) (1004 mV; orange dotted line). These predictions were tested by performing EPR-monitored radical equilibration studies on 2,3-F_2Y_{122}•-β2 (Figure S9). The observed populations of 2,3-F_2Y_{122}• and Y_{356}• correspond to

DOI: 10.1021/jacs.6b11011
J. Am. Chem. Soc. 2017, 139, 2994–3004

a $\Delta E^{\circ\prime}$(2,3-F_2Y_{122}• − Y_{356}•) of 47 ± 11 mV (pH 7.6, 25 °C). This results in a 27 ± 11 mV difference between 2,3,5-F_3Y_{122} (green line) and 2,3-F_2Y_{122} (1000 mV; orange solid line). Thus, the α_3X $\Delta E^{\circ\prime}$ (31 ± 2 mV) scale is preserved between 2,3,5-F_3Y_{122} and 2,3-F_2Y_{122} (27 ± 11 mV). This observation suggests that the reactions associated with the 2,3,5-F_3Y_{122} and 2,3-F_2Y_{122} redox cycles are similar and that both occur via Y(O•/O^-). Furthermore, since pK_a(2,3,5-F_3Y) < pK_a(2,3,6-F_3Y) < pK_a(3,5-F_2Y) < pK_a(2,3-F_2Y), we propose that Y_{122}(O•/O^-) is the operational redox couple in all four F_nY-substituted RNRs. It appears counterintuitive that $\Delta E^{\circ\prime}$(2,3-F_2Y_{122}(O•/O^-) − 2,3,5-F_3Y_{122}(O•/O^-)) is well predicted by the α_3X $\Delta E^{\circ\prime}$(pH 5.5) value and not by the $\Delta E^{\circ\prime}$ of the corresponding α_3X(O•/O^-) redox pairs (which equals −43 mV; Table S2). The simplest explanation is that F_nY_{122}(O•/O^-) is not a distinct redox couple but an interacting F_nY_{122}(O•/OH)/Fe1(H_2O/OH) "super" redox couple connected by a polarized H-bond or H-bonding network. Mössbauer data from the active ($\alpha 2\beta 2$/substrate/effector) wt system suggest that Y_{122} and Fe1 are H-bonded and that the phenol proton toggles back and forth depending on the redox state of Y_{122}.[64] In the F_nY_{122}-RNRs the phenol pK_a's are lower and we hypothesize that the proton is polarized toward Fe1 at all times. The polarized bond makes the system behave spectrally as a Y−O^- (as observed for reduced NO_2Y_{122}) but thermodynamically more as a Y(O•/OH) couple due to the H-bonding interactions between the phenol ring and Fe1.

Concluding Remarks. Site-specific incorporation of UAAs provides a powerful tool to study and engineer proteins and enzymes.[13] As the methodologies for UAA incorporation continue to improve, this approach is expanding in multiple directions in both basic science and applied research (e.g., ref 66). This report focuses on the use of F_nYs to perturb and characterize ET/PCET reactions in radical- and metallo-enzymes that use Y−O• in catalytic or long-range radical/hole transfer processes. Figure 1 shows F_nYs that have been used to study these types of reactions in enzymes.[11,17−23,63] Here we contribute data necessary for F_nY-based approaches to study protein redox chemistry. Until now, true thermodynamic potentials of the F_nYs have not been available for any medium, water or protein. Such data could be obtained by incorporating the F_nYs at site 32 in the well-structured α_3Y model protein (Figure 1). The F_nY_{32}−O• species are powerful oxidants. This issue was addressed by developing a protein film SW voltammetry approach that enabled collection of fully reversible voltammograms at uniquely high potentials. This approach generated α_3F_nY voltammograms of excellent quality and reproducibility. E°'s as high as +1200 mV vs the NHE could be determined with a precision of 2−3 mV. To provide a relevant comparison, the potential of the transient P_{680}^+/P_{680} redox pair in the PSII reaction center is estimated at ∼1170−1210 mV.[67] Thus, E°'s representing the very oxidizing edge of the biological redox scale could be reproduced in the 7.5 kDa α_3X model protein.

It has recently been suggested that aberrant reactive intermediates formed at buried metallo-cofactors may be removed via hole transfer along intramolecular Y/W chains linking the active site to the protein surface.[68] The F_nY_{32}(O•/OH) and F_nY_{32}(O•/O^-) redox couples span a considerable $\Delta E^{\circ\prime}$ range and, in combination with protein engineering,[13,14] could be used to test this hypothesis by altering the potentials of Ys along the proposed hole-transfer chains. These Y analogues could potentially also be used to map the thermodynamic profiles of radical migration processes observed in enzymes such as CcO, cyclooxygenase I and II and various peroxidases.[e.g.69] If engineered at active sites, the F_nYs could serve to estimate the potentials of metallo-oxidants too hot or too short-lived to be assessed by any other method. Additionally, and as demonstrated here, the α_3X-derived potentials can be used as a mechanistic tool to investigate the PCET vs ET nature of Y-based redox reactions.

■ ASSOCIATED CONTENT

Supporting Information

The Supporting Information is available free of charge on the ACS Publications website at DOI: 10.1021/jacs.6b11011.

Construction of the α_3F_nY expression system; protein expression and purification protocols; experimental conditions and settings for spectroscopic studies; analytical HPLC and MALDI-TOF evaluation of purified α_3F_nYs; representative urea-induced denaturation plots; CD and structural properties of the α_3F_nY proteins; SWV quasi-reversible maxima of α_3Y and 2MP-α_3C; representative protein film SW voltammograms and data processing details; Nernst equations and parameters used to model the α_3X E_{net} vs pH diagrams; current thermodynamic landscape of the RT pathway in *E. coli* class Ia RNR; radical equilibrium studies on F_nY-labeled RNRs. (PDF)

■ AUTHOR INFORMATION

Corresponding Author

*tommos@upenn.edu

ORCID

Kanchana R. Ravichandran: 0000-0001-5050-9719
Daniel G. Nocera: 0000-0001-5055-320X
JoAnne Stubbe: 0000-0001-8076-4489
Cecilia Tommos: 0000-0001-8095-8873

Notes

The authors declare no competing financial interest.

■ ACKNOWLEDGMENTS

Funding was provided by National Institutes of Health grants GM47274 (D.G.N), GM29595 (J.S.) and GM079190 (C.T.)

■ REFERENCES

(1) Marcus, R. A.; Sutin, N. *Biochim. Biophys. Acta, Rev. Bioenerg.* **1985**, *811*, 265−322.

(2) (a) Beratan, D. N.; Onuchic, J. N.; Winkler, J. R.; Gray, H. B. *Science* **1992**, *258*, 1740−1741. (b) Gray, H. B.; Winkler, J. R. *Q. Rev. Biophys.* **2003**, *36*, 341−372. (c) Winkler, J. R.; Gray, H. B. *Chem. Rev.* **2014**, *114*, 3369−3380.

(3) (a) Moser, C. C.; Keske, J. M.; Warncke, K.; Farid, R. S.; Dutton, P. L. *Nature* **1992**, *355*, 796−802. (b) Page, C. C.; Moser, C. C.; Chen, X.; Dutton, P. L. *Nature* **1999**, *402*, 47−52. (c) Moser, C. C.; Anderson, J. L. R.; Dutton, P. L. *Biochim. Biophys. Acta, Bioenerg.* **2010**, *1797*, 1573−1586.

(4) (a) Cukier, R. I.; Nocera, D. G. *Annu. Rev. Phys. Chem.* **1998**, *49*, 337−369. (b) Reece, S. Y.; Nocera, D. G. *Annu. Rev. Biochem.* **2009**, *78*, 673−699.

(5) (a) Huynh, M. H.; Meyer, T. J. *Chem. Rev.* **2007**, *107*, 5004−5064. (b) Weinberg, D. R.; Gagliardi, C. J.; Hull, J. F.; Murphy, C. F.; Kent, C. A.; Westlake, B. C.; Paul, A.; Ess, D. H.; McCafferty, D. G.; Meyer, T. J. *Chem. Rev.* **2012**, *112*, 4016−4093.

(6) Hammes-Schiffer, S.; Stuchebrukhov, A. A. *Chem. Rev.* **2010**, *110*, 6939−6960.

DOI: 10.1021/jacs.6b11011
J. Am. Chem. Soc. 2017, 139, 2994−3004

(7) (a) Mayer, J. M. *Annu. Rev. Phys. Chem.* **2004**, *55*, 363−390. (b) Warren, J. J.; Tronic, T. A.; Mayer, J. M. *Chem. Rev.* **2010**, *110*, 6961−697001.
(8) Migliore, A.; Polizzi, N. F.; Therien, M. J.; Beratan, D. N. *Chem. Rev.* **2014**, *114*, 3381−3465.
(9) (a) Vinyard, D. J.; Ananyev, G. M.; Dismukes, G. C. *Annu. Rev. Biochem.* **2013**, *82*, 577−606. (b) Shen, J.-R. *Annu. Rev. Plant Biol.* **2015**, *66*, 23−48.
(10) (a) Kaila, V. R. I.; Verkhovsky, M. I.; Wikström, M. *Chem. Rev.* **2010**, *110*, 7062−7081. (b) Blomberg, M. R. A. *Biochemistry* **2016**, *55*, 489−500.
(11) Minnihan, E. C.; Nocera, D. G.; Stubbe, J. *Acc. Chem. Res.* **2013**, *46*, 2524−2535.
(12) Stubbe, J.; Nocera, D. G.; Yee, C. S.; Chang, M. C. Y. *Chem. Rev.* **2003**, *103*, 2167−2201.
(13) Liu, C. C.; Schultz, P. G. *Annu. Rev. Biochem.* **2010**, *79*, 413−444.
(14) Minnihan, E. C.; Young, D. D.; Schultz, P. G.; Stubbe, J. *J. Am. Chem. Soc.* **2011**, *133*, 15942−15945.
(15) Kim, K.; Cole, P. A. *J. Am. Chem. Soc.* **1998**, *120*, 6851−6858.
(16) Seyedsayamdost, M. R.; Reece, S. Y.; Nocera, D. G.; Stubbe, J. *J. Am. Chem. Soc.* **2006**, *128*, 1569−1579.
(17) Ravichandran, K. R.; Minnihan, E. C.; Wei, Y.; Nocera, D. G.; Stubbe, J. *J. Am. Chem. Soc.* **2015**, *137*, 14387−14395.
(18) Oyala, P. H.; Ravichandran, K. R.; Funk, M. A.; Stucky, P. A.; Stich, T. A.; Drennan, C. L.; Britt, R. D.; Stubbe, J. *J. Am. Chem. Soc.* **2016**, *138*, 7951−7964.
(19) (a) Holder, P. G.; Pizano, A. A.; Anderson, B. L.; Stubbe, J.; Nocera, D. G. *J. Am. Chem. Soc.* **2012**, *134*, 1172−1180. (b) Olshansky, L.; Pizano, A. P.; Wei, Y.; Stubbe, J.; Nocera, D. G. *J. Am. Chem. Soc.* **2014**, *136*, 16210−16216. (c) Song, D. Y.; Pizano, A. A.; Holder, P. G.; Stubbe, J.; Nocera, D. G. *Chem. Sci.* **2015**, *6*, 4519−4524.
(20) Olshansky, L.; Stubbe, J.; Nocera, D. G. *J. Am. Chem. Soc.* **2016**, *138*, 1196−1205.
(21) Rappaport, F.; Boussac, A.; Force, D. A.; Peloquin, J.; Brynda, M.; Sugiura, M.; Un, S.; Britt, R. D.; Diner, B. A. *J. Am. Chem. Soc.* **2009**, *131*, 4425−4433.
(22) Yu, Y.; Lv, X.; Li, J.; Zhou, Q.; Cui, C.; Hosseinzadeh, P.; Mukherjee, A.; Nilges, M. J.; Wang, J.; Lu, Y. *J. Am. Chem. Soc.* **2015**, *137*, 4594−4597.
(23) Yu, Y.; Zhou, Q.; Wang, L.; Liu, X.; Zhang, W.; Hu, M.; Dong, J.; Li, J.; Lv, X.; Ouyang, H.; Li, H.; Gao, F.; Gong, W.; Lu, Y.; Wang, J. *Chem. Sci.* **2015**, *6*, 3881−3885.
(24) Hosseinzadeh, P.; Lu, Y. *Biochim. Biophys. Acta, Bioenerg.* **2016**, *1857*, 557−581.
(25) Tommos, C.; Skalicky, J. J.; Pilloud, D. L.; Wand, A. J.; Dutton, P. L. *Biochemistry* **1999**, *38*, 9495−9507.
(26) Westerlund, K.; Berry, B. W.; Privett, H. K.; Tommos, C. *Biochim. Biophys. Acta, Bioenerg.* **2005**, *1707*, 103−116.
(27) Dai, Q. H.; Tommos, C.; Fuentes, E. J.; Blomberg, M. R. A.; Dutton, P. L.; Wand, A. J. *J. Am. Chem. Soc.* **2002**, *124*, 10952−10953.
(28) Tommos, C.; Valentine, K. G.; Martínez-Rivera, M. C.; Liang, L.; Moorman, V. R. *Biochemistry* **2013**, *52*, 1409−1418.
(29) Glover, S. D.; Jorge, C.; Liang, L.; Valentine, K. G.; Hammarström, L.; Tommos, C. *J. Am. Chem. Soc.* **2014**, *136*, 14039−14051.
(30) Ravichandran, K. R.; Liang, L.; Stubbe, J.; Tommos, C. *Biochemistry* **2013**, *52*, 8907−8915.
(31) Hay, S.; Westerlund, K.; Tommos, C. *Biochemistry* **2005**, *44*, 11891−11902.
(32) Martínez-Rivera, M. C.; Berry, B. W.; Valentine, K. G.; Westerlund, K.; Hay, S.; Tommos, C. *J. Am. Chem. Soc.* **2011**, *133*, 17786−17795.
(33) Berry, B. W.; Martínez-Rivera, M. C.; Tommos, C. *Proc. Natl. Acad. Sci. U. S. A.* **2012**, *109*, 9739−9743.
(34) (a) Armstrong, F. A.; Wilson, G. S. *Electrochim. Acta* **2000**, *45*, 2623−2645. (b) Armstrong, F. A.; Camba, R.; Heering, H. A.; Hirst, J.; Jeuken, L. J. C.; Jones, A. K.; Léger, C.; McEvoy, J. P. *Faraday Discuss.* **2000**, *116*, 191−203. (c) Léger, C.; Bertrand, P. *Chem. Rev.* **2008**, *108*, 2379−2438.
(35) Simon, J.; Salzbrunn, S.; Prakash, G. K. S.; Petasis, N. A.; Olah, G. A. *J. Org. Chem.* **2001**, *66*, 633−634.
(36) Chen, H.; Gollnick, P.; Phillips, R. S. *Eur. J. Biochem.* **1995**, *229*, 540−549.
(37) Seyedsayamdost, M. R.; Yee, C. S.; Stubbe, J. *Nat. Protoc.* **2007**, *2*, 1225−1235.
(38) Bendezú, F. O.; Hale, C. A.; Bernhardt, T. G.; de Boer, P. A. J. *EMBO J.* **2009**, *28*, 193−204.
(39) Salwiczek, M.; Nyakatura, E. K.; Gerling, U. I. M.; Ye, S.; Koksch, B. *Chem. Soc. Rev.* **2012**, *41*, 2135−2171.
(40) Buer, B. C.; Meagher, J. L.; Stuckey, J. A.; Marsh, E. N. G. *Proc. Natl. Acad. Sci. U. S. A.* **2012**, *109*, 4810−4815.
(41) Mortenson, D. E.; Satyshur, K. A.; Guzei, I. A.; Forest, K. T.; Gellman, S. H. *J. Am. Chem. Soc.* **2012**, *134*, 2473−2476.
(42) Tang, Y.; Ghirlanda, G.; Vaidehi, N.; Kua, J.; Mainz, D. T.; Goddard, W. A., III; DeGrado, W. F.; Tirrell, D. A. *Biochemistry* **2001**, *40*, 2790−2796.
(43) Clark, G. A.; Baleja, J. D.; Kumar, K. *J. Am. Chem. Soc.* **2012**, *134*, 17912−17921.
(44) Osteryoung, J.; O'Dea, J. J. In *Electroanalytical Chemistry*; Bard, A. J., Ed.; Marcel Dekker: New York, 1986; Vol. *14*, pp 209−308.
(45) (a) Mirčeski, V.; Komorsky-Lovrić, Š.; Lovrić, M. Square-wave voltammetry: Theory and applications. In *Monographs in Electrochemistry*; Scholz, F., Ed.;Springer-Verlag: Berlin, Germany, 2007. (b) Mirčeski, V.; Gulaboski, R.; Lovrić, M.; Bogeski, I.; Kappl, R.; Hoth, M. *Electroanalysis* **2013**, *25*, 2411−2422.
(46) Mahmoudi, L.; Kissner, R.; Nauser, T.; Koppenol, W. H. *Biochemistry* **2016**, *55*, 2849−2856.
(47) (a) Lovrić, M.; Komorsky-Lovrić, Š. *J. Electroanal. Chem. Interfacial Electrochem.* **1988**, *248*, 239−253. (b) Komorsky-Lovrić, Š.; Lovrić, M. *J. Electroanal. Chem.* **1995**, *384*, 115−122. (c) Komorsky-Lovrić, Š.; Lovrić, M. *Anal. Chim. Acta* **1995**, *305*, 248−255.
(48) (a) Reeves, J. H.; Song, S.; Bowden, E. F. *Anal. Chem.* **1993**, *65*, 683−688. (b) O'Dea, J. J.; Osteryoung, J. G. *Anal. Chem.* **1993**, *65*, 3090−3097.
(49) Wu, Y.; Fried, S. D.; Boxer, S. G. *Biochemistry* **2015**, *54*, 7110−7119.
(50) (a) Jovanovic, S. V.; Harriman, A.; Simic, M. G. *J. Phys. Chem.* **1986**, *90*, 1935−1939. (b) Lind, J.; Eriksen, T. E.; Merényi, G. *J. Am. Chem. Soc.* **1990**, *112*, 479−482.
(51) DeFelippis, M. R.; Murthy, C. P.; Faraggi, M.; Klapper, M. H. *Biochemistry* **1989**, *28*, 4847−4853.
(52) Folkes, L. K.; Trujillo, M.; Bartesaghi, S.; Radi, R.; Wardman, P. *Arch. Biochem. Biophys.* **2011**, *506*, 242−249.
(53) Harriman, A. *J. Phys. Chem.* **1987**, *91*, 6102−6104.
(54) DeFelippis, M. R.; Murthy, C. P.; Broitman, F.; Weinraub, D.; Faraggi, M.; Klapper, M. H. *J. Phys. Chem.* **1991**, *95*, 3416−3419.
(55) Yee, C. S.; Seyedsayamdost, M. R.; Chang, M. C. Y.; Nocera, D. G.; Stubbe, J. *Biochemistry* **2003**, *42*, 14541−14552.
(56) Armstrong, D. A.; Huie, R. E.; Koppenol, W. H.; Lymar, S. V.; Merényi, G.; Neta, P.; Ruscic, B.; Stanbury, D. M.; Steen Steenken, S.; Wardman, P. *Pure Appl. Chem.* **2015**, *87*, 1139−1150.
(57) (a) Prütz, W. A.; Butler, J.; Land, E. J. *Int. J. Radiat. Biol. Relat. Stud. Phys., Chem. Med.* **1983**, *44*, 183−196. (b) Hawkins, C. L.; Davies, M. J. *Biochim. Biophys. Acta, Bioenerg.* **2001**, *1504*, 196−219.
(58) Costentin, C.; Louault, C.; Robert, M.; Savéant, J.-M. *Proc. Natl. Acad. Sci. U. S. A.* **2009**, *106*, 18143−18148.
(59) Nicholson, R. S. *Anal. Chem.* **1965**, *37*, 667−671.
(60) Nick, T. U.; Lee, W.; Kassmann, S.; Neese, F.; Stubbe, J.; Bennati, M. *J. Am. Chem. Soc.* **2015**, *137*, 289−298.
(61) Yokoyama, K.; Uhlin, U.; Stubbe, J. *J. Am. Chem. Soc.* **2010**, *132*, 15368−15379.
(62) Yokoyama, K.; Smith, A. A.; Corzilius, B.; Griffin, R. G.; Stubbe, J. *J. Am. Chem. Soc.* **2011**, *133*, 18420−18432.
(63) Ravichandran, K. R.; Taguchi, A. T.; Wei, Y.; Tommos, C.; Nocera, D. G.; Stubbe, J. *J. Am. Chem. Soc.* **2016**, *138*, 13706−13716.

DOI: 10.1021/jacs.6b11011
J. Am. Chem. Soc. 2017, 139, 2994−3004

(64) Wörsdörfer, B.; Conner, D. A.; Yokoyama, K.; Livada, J.; Seyedsayamdost, M.; Jiang, W.; Silakov, A.; Stubbe, J.; Bollinger, J. M., Jr.; Krebs, C. *J. Am. Chem. Soc.* **2013**, *135*, 8585−8593.
(65) Yokoyama, K.; Uhlin, U.; Stubbe, J. *J. Am. Chem. Soc.* **2010**, *132*, 8385−8397.
(66) (a) Kim, C. H.; Axup, J. Y.; Schultz, P. G. *Curr. Opin. Chem. Biol.* **2013**, *17*, 412−419. (b) Hallam, T. J.; Wold, E.; Wahl, A.; Smider, V. V. *Mol. Pharmaceutics* **2015**, *12*, 1848−1862. (c) Quast, R. B.; Mrusek, D.; Hoffmeister, C.; Sonnabend, A.; Kubick, S. *FEBS Lett.* **2015**, *589*, 1703−1712.
(67) (a) Shibamoto, T.; Kato, Y.; Sugiura, M.; Watanabe, T. *Biochemistry* **2009**, *48*, 10682−10684. (b) Nilsson, H.; Cournac, L.; Rappaport, F.; Messinger, J.; Lavergne, J. *Biochim. Biophys. Acta, Bioenerg.* **2016**, *1857*, 23−33.
(68) (a) Gray, H. B.; Winkler, J. R. *Proc. Natl. Acad. Sci. U. S. A.* **2015**, *112*, 10920−10925. (b) Winkler, J. R.; Gray, H. B. *Q. Rev. Biophys.* **2015**, *48*, 411−420.
(69) (a) Yu, M. A.; Egawa, T.; Shinzawa-Itoh, K.; Yoshikawa, S.; Guallar, V.; Yeh, S.-R.; Rousseau, D. L.; Gerfen, G. J. *J. Am. Chem. Soc.* **2012**, *134*, 4753−4761. (b) Tsai, A.-L.; Kulmacz, R. J. *Arch. Biochem. Biophys.* **2010**, *493*, 103−124. (c) Ranguelova, K.; Girotto, S.; Gerfen, G. J.; Yu, S.; Suarez, J.; Metlitsky, L.; Magliozzo, R. S. *J. Biol. Chem.* **2007**, *282*, 6255−6264. (d) Miner, K. D.; Pfister, T. D.; Hosseinzadeh, P.; Karaduman, N.; Donald, L. J.; Loewen, P. C.; Lu, Y.; Ivancich, A. *Biochemistry* **2014**, *53*, 3781−3789.

DOI: 10.1021/jacs.6b11011
J. Am. Chem. Soc. 2017, 139, 2994−3004